Appl. Phys. B 87, 333–339 (2007)
DOI: 10.1007/s00340-007-2597-7

Applied Physics B
Lasers and Optics

L. SCHNEIDER
H.J. SCHMID
W. PEUKERT✉

Influence of particle size and concentration on the second-harmonic signal generated at colloidal surfaces

Institute of Particle Technology, Friedrich-Alexander University Erlangen-Nuremberg,
Cauer Str. 4, 91058 Erlangen, Germany

Received: 6 September 2006/
Revised version: 19 December 2006
Published online: 24 March 2007 •

ABSTRACT Second harmonic generation (SHG) spectroscopy is a recently developed technique for the investigation of surface properties of particles. To apply the method to technical colloidal systems, the dependences of several experimental parameters on the signal have to be studied. In this work the influence of particle concentration on the SHG signal from the surfaces of colloids (polystyrene beads in a size range of 0.1 μm to 2.9 μm) is investigated. A simple model, based on Lambert–Beer's law, to describe the measured dependences is derived. The model agrees with the experimental observations for particles smaller 1.1 μm and with a small modification also for larger particles. Based on the new model an analytical equation for determining the optimum concentration, where highest signals in colloidal SHG spectroscopy measurements are obtained, is derived.

PACS 42.25.Fx; 42.65.-k; 82.70.Dd

1 Introduction

Manufacturing and handling of colloidal particles is vigorously determined by the particle interface properties. Coagulation and stabilization, rheology, filtration and many other processes are influenced by particle interactions and thus by the surface properties of the particles. For example, nanoparticle production by comminution in stirred media mills finds a lower limit for product particle size when reaching an equilibrium of breakage and agglomeration [1]. Changing the surface charge of the particles or adsorbing steric polymers on the surfaces increases the suspension stability with respect to agglomeration. Thus, lower particle sizes can be obtained. For controlling such processes it would be convenient to measure the particle surface properties during the production processes. The only technique that has the potential to study chemistry and physics on such buried surfaces and even with high time resolution is nonlinear optical spectroscopy, i.e. second harmonic generation (SHG) and sum frequency generation (SFG) spectroscopy [2].

Second order nonlinear effects are electrically dipole forbidden in centrosymmetric media. At an interface between two such media there is always a symmetry break leading to a nonvanishing nonlinear susceptibility $\chi^{(2)}$, which gives rise to a nonlinear signal. In SHG this is a frequency-doubled signal with respect to the incident light. SHG spectroscopy was developed in the early 1980s [2, 3] and has become an established technique for the investigation of planar surfaces. The advantages are the intrinsic surface specificity, the applicability to all optically accessible surfaces and the high temporal resolution. In 1996, Wang et al. showed the possibility of applying the method to the investigation of colloidal surfaces [4]. Since then the technique has proven to be a powerful method for characterizing adsorption processes on polymer beads [4–8], clay particles [9] and emulsions [10]. The surface charge of colloidal particles was also observed by electric field induced SHG (EFISHG) [11, 12] as well as charge-transfer processes of semiconductor particles [13].

All these experiments have been realized at 'model' systems like monodisperse spheres at fixed number concentration. For establishing the method and applying it to technical suspensions, several experimental parameters have to be taken into account. A very important one is the particle concentration: in a common transmission setup, the SH signal should rise with increasing number of particles. At the same time higher absorption and scattering of the incident as well as the generated light should decrease the detected signal. For the characterization of surface properties of particles in real systems this concentration dependence has to be known and taken into account. In the following some experimental results about the SHG concentration dependence of polystyrene (PS) microspheres with different diameters will be shown. A simple model based on Lambert–Beer's extinction behavior is developed to describe the concentration dependence of the SHG signal theoretically. This model allows a prediction of the concentration behavior for a certain suspension if the linear extinction coefficients at the wavelengths of interest are known. These can be determined by simple UV-Vis measurements or by applying Mie's theory. To our best knowledge, we are the first who studied in detail the influence of concentration on the SHG signal generated at surfaces of particles.

2 Theoretical description of the concentration dependence

The electric field of the generated SH signal ($E_{2\omega}$) is proportional to the square of the incident E field (E_{ω}) and

✉ Fax: +49-9131-8529402, E-mail: w.peukert@lfg.uni-erlangen.de

the second order nonlinear susceptibility $\chi^{(2)}$:

$$E_{2\omega} \propto \chi^{(2)} E_{\omega}^2 . \tag{1}$$

In this work, independence of the signals generated by different particle surfaces and a homogeneous particle distribution are assumed. Thus, we can introduce an effective nonlinear susceptibility β. The total SHG intensity $I_{2\omega}^{\mathrm{p}}(\boldsymbol{r})$ generated at the interface of one particle, located at the position $\boldsymbol{r}$ somewhere within the suspension, which is illuminated by light of intensity $I_{\omega}(\boldsymbol{r})$, will then be described by

$$I_{2\omega}^{\mathrm{p}}(\boldsymbol{r}) = \beta^2 I_{\omega}^2(\boldsymbol{r}) . \tag{2}$$

In a colloidal suspension the incident light is attenuated by the particles due to scattering and to some extent by adsorption (if the influence of the solvent is neglected). For systems with moderate concentrations this attenuation behavior can be described by Lambert–Beer's law as a function of the position (z) in the propagation direction. $I_{\omega}(\boldsymbol{r})$ then becomes, in the case of a TEM_{00} Gaussian beam profile for the incident light,

$$I_{\omega}(\boldsymbol{r}(x,y,z)) = I_0 \left(\frac{w_0}{w(z)}\right)^2 \mathrm{e}^{-2\frac{x^2+y^2}{w(z)^2}} \mathrm{e}^{-\alpha_{\omega} c (z-z_0)} , \tag{3}$$

with the intensity of the incident light I_0, the linear extinction coefficient α_{ω} for the incident wavelength ($\lambda = 846$ nm) in the forward direction, the number concentration c of the particles and the position of the cuvette entrance z_0. The beam waist w_0 at the focus and $w(z)$ at the position z depend on the focal length f of the applied lens.

The generated light will be attenuated by scattering as well, when passing the remaining path within the suspension. We also assume an exponential behavior. However, the extinction factor will surely be lower than the linear extinction coefficient for the half wavelength $\alpha_{2\omega}$ ($\lambda = 423$ nm): not the light in the forward direction (which is actually zero [5, 14]) but in contrast a large fraction of the scattered signal is detected (see the setup below with an angle of acceptance of about 60°). Therefore, we assume an extinction coefficient $\alpha_{2\omega}/t$ with a factor t that has to be determined. In our work the values of t will be obtained by a numerical fit of (6) to the experimental data. But, in general, it should be possible to determine the value of t theoretically, as well, if the scattering behavior of the generated nonlinear light within the cuvette was known. In this case, taking into account the experimental aperture, the part of the light reaching the detector could be calculated accurately. First experimental and theoretical works on the nonlinear scattering behavior in colloids can be found in the literature [5, 14–18].

If t is known, the detected nonlinear signal generated by one particle will therefore be

$$I_{\mathrm{det}}^{\mathrm{p}} = I_{2\omega}^{\mathrm{p}} \mathrm{e}^{-\frac{\alpha_{2\omega}}{t} c (z_1 - z)} , \tag{4}$$

with the position of the cuvette exit z_1. To obtain the total SHG signal generated in the suspension, the individual signals of all particles have to be summed. Since the number of particles in the volume element $\mathrm{d}N$ is given by $\mathrm{d}N = c\mathrm{d}V$, the following integral has to be solved:

$$I_{2\omega} = \beta^2 c \int_{-\infty}^{\infty}\int_{-\infty}^{\infty}\int_{z_0}^{z_1} I_{\omega}(\boldsymbol{r})^2 \, \mathrm{e}^{-\frac{\alpha_{2\omega}}{t} c (z_1 - z)} \mathrm{d}x\mathrm{d}y\mathrm{d}z . \tag{5}$$

Performing the integration over $\mathrm{d}x$ and $\mathrm{d}y$ leads to

$$I_{2\omega} = \beta^{*2} c \int_{z_0}^{z_1} \frac{w_0^4}{w^2(z)} \mathrm{e}^{-2\alpha_{\omega} c (z - z_0)} \mathrm{e}^{-\frac{\alpha_{2\omega}}{t} c (z_1 - z)} \mathrm{d}z , \tag{6}$$

with $\beta^* = \dfrac{\pi}{4} I_0^2 \beta$.

3 Experimental

To assure a high peak power and a low absorption, short laser pulses are usually applied for SHG experiments. We used a Ti:sapphire femtosecond laser (Millenia-pumped Tsunami, Spectra Physics), which provides pulses of approximately 60 fs at a repetition rate of 82 MHz. The wavelength is tunable from 700 to 1000 nm. All experiments in this work were performed at a wavelength of 846 nm and a mean power of 1.4 W. We used a transmission setup, schematically shown in Fig. 1. After blocking SH signals, possibly generated at the mirror surfaces before reaching the lens by a glass filter (RG695), the beam is focused into a sample cell (rectangular, 2-mm path length). The scattered light as well as the scattered signal are collimated by a second lens which is situated in the forward direction. The angle of acceptance is about 60°. A low-pass glass filter (BG38) separates the SH light from the

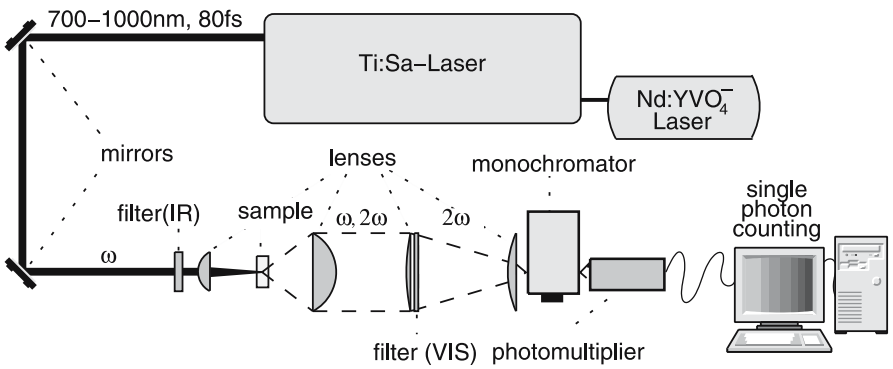

FIGURE 1 Transmission setup of the SHG spectrometer

incident light. After a beam-size reduction and focusing into a monochromator for a more accurate separation, the signal is detected by a photomultiplier tube (Hamamatsu R-7205-01) and processed by a photon counter. The signals are finally recorded by a computer. All SHG experiments as well as the calculations were performed for vertically polarized incident light. Since in SHG spectroscopy at colloidal surfaces the interesting quantity is the intensity, the total generated light was detected independently from the polarization state. However, all the ideas applied in this work to describe the signal behavior for one special polarization configuration are expected to be transferable to any different configuration without loss of generality.

For measuring the linear attenuation behavior of the investigated suspensions, UV-Vis transmission experiments were performed. The scanning option of a Cary 100 from Variant was applied. Thus, the ratio of transmitted and incident light as a function of wavelength was measured. Scans were performed from 400 nm to 850 nm. The values at 423 nm and 846 nm, respectively, were chosen to calculate the attenuation coefficient due to Lambert–Beer's law. Rectangular cuvettes of 2-mm path lengths were used.

The investigated colloids consisted of polystyrene (PS) microspheres of different diameters from Polysciences with plain surfaces (polybeads) in a size range from 107 nm to 2.98 μm (see Table 1). Concentrations of the original suspensions were between 2.5 and 2.7 vol.%. On the particle surfaces malachite green (MG) hydrochloride (from Aldrich without further purification), a cationic dye with a high nonlinearity, was adsorbed. Therefore, a defined amount of the original suspensions was mixed with a solution of MG. The particle as well as the MG concentration were varied in the experiments for different particle sizes. The MG molecules lead to SH signal increases up to 1000 times in comparison to the plain surfaces [4], whereas the normalized trend for the particle concentration dependence is not influenced, as will be shown below. Thus, the signal to noise ratio is strongly enhanced and measurement time can be reduced. Detailed information about the investigation of MG adsorption on PS particles by SHG can be found in the literature [4, 5, 8, 10].

The stability of the suspensions was validated by dynamic light scattering (DLS) particle sizing in a Malvern Zetasizer Nano, before and after the SHG experiments. These experiments showed a narrow size distribution for all particles.

Diameter [μm]	Variance [μm]	rms [%] (norm. intensity)	rms new [%] (norm. intensity)
0.107	0.005	4.3	–
0.203	0.010	3.1	–
0.356	0.014	7.7	–
0.465	0.011	8.1	–
0.535	0.010	7.7	–
0.771	0.025	6.3	–
1.093	0.032	4.9	–
1.826	0.046	27.6	6.3
2.979	0.139	17.1	3.4

TABLE 1 Particle diameters and variances of the investigated PS particles. Additionally, the rms values as a quantity for the degree of correspondence between experimental data and calculated trends in the concentration behavior are listed

To directly compare SHG and UV-Vis measurements all experiments were performed in rectangular cuvettes with a path length of 2 mm. After measuring the SHG signal the sample was removed from the cell and diluted with millipore water to obtain a lower particle concentration. By this procedure a well-dispersed suspension is guaranteed for each sample. Measurements were performed within the first 30 s after filling the cuvette. Thus, changes in signal with time due to heating effects or particle sedimentation were avoided. Effectively, no significant signal changes could be noticed when measuring the sample for several minutes.

4 Results and discussion

4.1 UV-Vis *measurements*

Figure 2 shows exemplary UV-Vis spectra of the 0.771-μm PS particles for different number concentrations in the wavelength range from 400 nm to 850 nm. At high concentrations a small absorption peak at 623 nm resulting from a two-photon resonance of the MG can be observed, whereas no influence of MG absorption can be seen at the wavelengths of interest (846 nm and 423 nm). The corresponding extinction behavior is illustrated in Fig. 3. The logarithmic

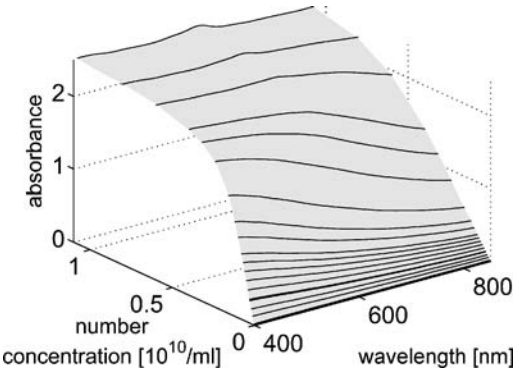

FIGURE 2 UV-Vis extinction experiment for 0.771-μm PS particles with MG

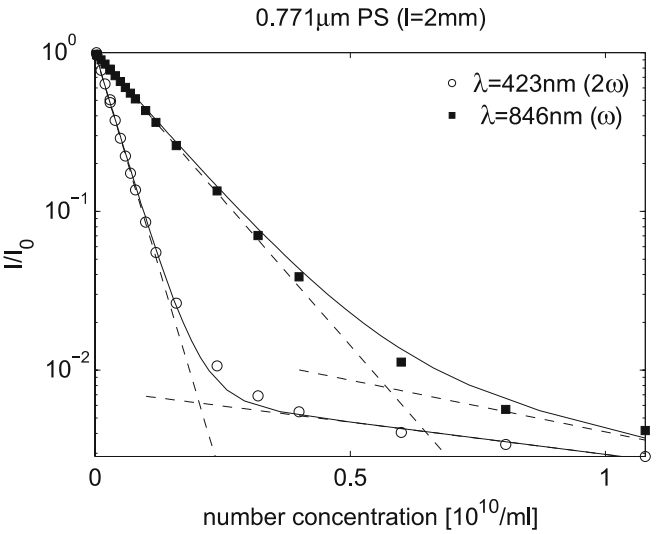

FIGURE 3 Extinction behavior at the wavelengths corresponding to ω (846 nm) and 2ω (423 nm) in a 2-mm cuvette

scale demonstrates the exponential Lambert–Beer decay (dotted line) up to a certain number concentration (0.5×10^{10} /ml for 846 nm, 0.2×10^{10} /ml for 423 nm). At higher concentrations the curve deviates from this behavior due to multiple scattering leading to another exponential decay. The total extinction behavior can thus be described by the sum of these two exponential functions (solid line). Figure 4 shows that for higher concentrations the exact solution decays slightly more weakly than for the Lambert–Beer assumption. Nevertheless, the difference is not as strong as one would expect due to the significant change in slope that can be observed in Fig. 3.

4.2 *Comparison of theory and experiments*

Since no absorption of the MG at the wavelengths of interest can be observed, only β^* in (6) depends on the MG concentration, and thus only the absolute intensity values.

Figure 4 shows the normalized SHG intensity of the 0.771-μm PS particles as a function of particle concentration for different amounts of MG and two different focusing lenses with 100 mm and 50 mm focal lengths. The figure verifies the statement that the normalized concentration dependence is not influenced by the addition of MG to the suspension nor by the focusing, since the trends of all four experiments coincide. The results shown for the 0.771-μm particles are valid for all investigated particle sizes, as clearly proven by the experiment.

The figure shows further a good agreement between the experimental concentration dependence and the calculated one (by numerical integration of (6)) and determining the factor t by a numerical fit. The obtained values of t for the different particle sizes, thereby, all lie between 4.5 and 6. No general dependence between this factor and the corresponding particle size could be observed. In fact, using the mean value of $t = 5.2$ for calculating the concentration dependence with (6) also matches well the trend of the experimental data.

The absolute root mean square (rms) values for the deviations between the measured and the calculated data points, which are listed in Table 1, confirm a similar matching for other particle sizes as long as the diameter is below 1.1 μm. The corresponding trends can be found in the appendix of this work.

The concentration behavior of the linear signal was investigated with the same setup, detecting only light of the original wavelength (corresponding to ω) after exchanging the blue glass filter by an infrared filter (which further blocked the central cone of the signal) and adjusting the monochromator to 846 nm. The trend can be seen in Fig. 5. To apply the model from above to the linear behavior, the extinction factor for the generated light ($\alpha_{2\omega}$) has to be substituted by the linear one (α_ω). The dependence from the incident intensity is further linear (not quadratic). An interesting point is the resulting value for the parameter t ($t = 1.8$) in comparison with the value for the SHG experiment ($t = 5.6$). This shows the strong differences in the nonlinear and linear scattering behavior. Details about the nonlinear scattering behavior can be found in Fig. 12.

For larger particles the assumption in the derivation of (6) that scattered light does not contribute to the generation of SH light is not applicable any more. Due to Mie theory most of the light scattered by 'larger' particles will propagate in almost the forward direction. Furthermore, the intensity of this forward-scattered light from larger particles will be higher than in the case of smaller particles. Thus, the scattered light will also produce nonlinear signals. This idea can be included in (6) by assuming a lower extinction coefficient (α_ω) for the incoming light. A numerical fit revealed that the extinction factors of the 1.8-μm and the 2.9-μm particles have to be divided by 3.5 to obtain a good agreement between the calculated trend and experimental data again (see Fig. 6 and the resulting rms values (rms new) in Table 1). It is somewhat surprising that the values

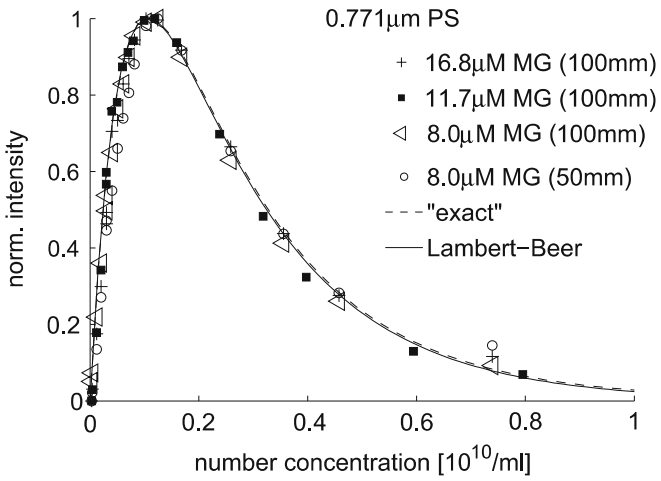

FIGURE 4 Experimental data for the concentration dependence for 0.771-μm PS particles for different MG concentrations of the basic solution in a 2-mm cuvette. The *lines* represent the calculated trends using the Lambert–Beer extinction for the intensities and the 'exact' extinction behavior

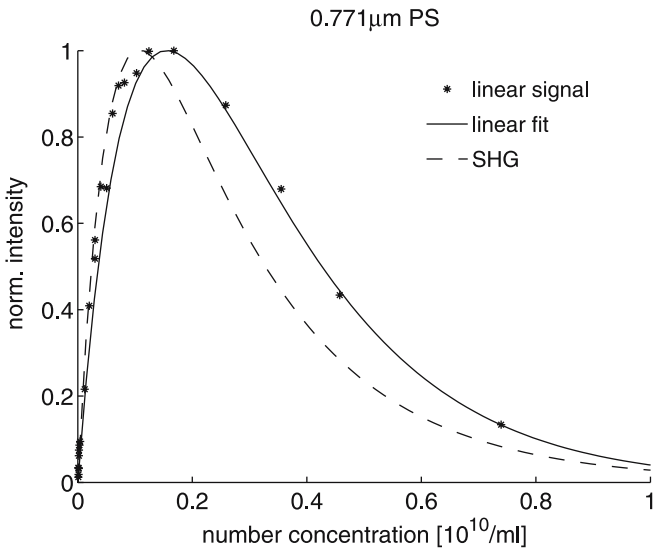

FIGURE 5 Comparison of the concentration behaviors of the scattered linear signal and the SHG signal measured with the same transmission setup. The experiment was performed for 0.771-μm PS particles in a 8 μM MG basic solution (2-mm cuvette)

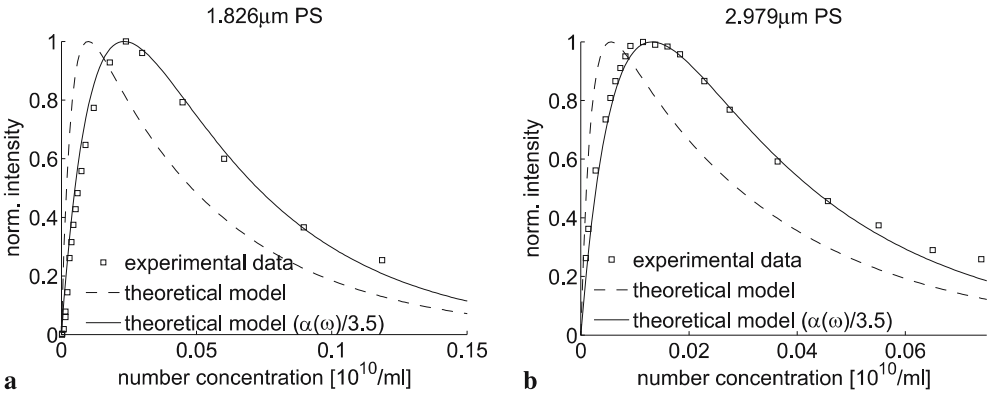

FIGURE 6 Concentration dependence for 'large' particles. (**a**) 1.826-μm PS particles, (**b**) 2.979-μm PS particles. The *dashed lines* represent the calculated trends with the extinction factor (α_ω) in the forward direction. The *solid lines* result from the same calculation but with a reduced extinction factor ($\alpha_\omega/3.5$)

for the reduction of the extinction coefficients for these two particle sizes coincide, especially because a jump from the factor 1 (1.1-μm particles) to the factor 3.5 (2.8-μm particles) is observed. To obtain a deeper insight into this issue, the behavior in the intermediate size range has to be investigated.

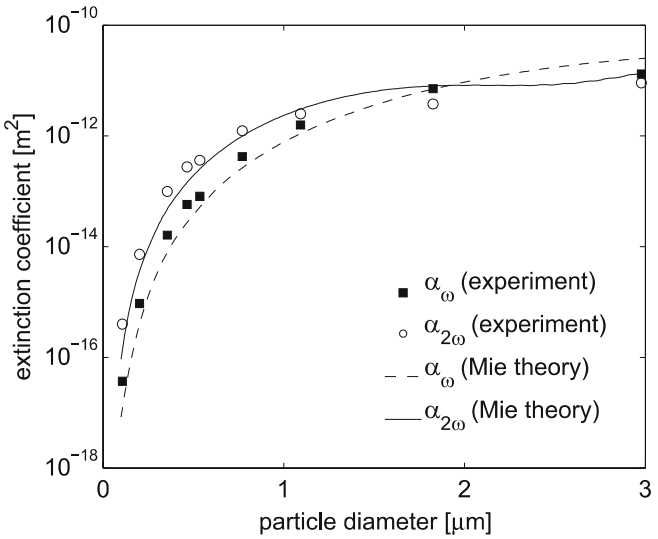

FIGURE 7 Comparison of experimentally obtained and calculated (Mie theory) extinction coefficients for the 0.771-μm-sized particles with refractive index of $1.591 + 0.003$i

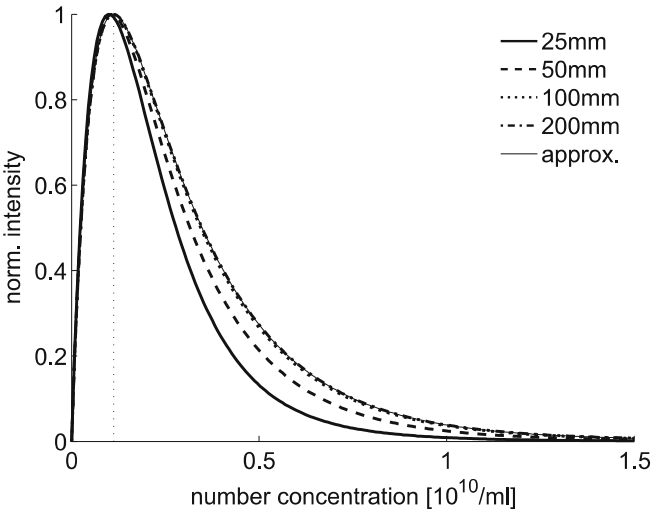

FIGURE 8 Comparison of the approximated (8) and the 'exact' solution of (6) for different focal lengths of the lens

4.3 *Extinction coefficients by Mie theory*

By applying the Mie theory the extinction coefficients for the investigated colloidal systems can be calculated for the accordant wavelengths and particle sizes, without performing any experiments (a refractive index for PS of $1.591 + 0.003$i was assumed). Figure 7 illustrates a good agreement between the experimentally obtained coefficients and the theoretically derived ones for the particles of 0.771-μm diameter. Therefore, if the factor t in (6) is known for a certain particle system the concentration behavior for the system can be predicted theoretically.

4.4 *Determining the optimal concentration*

By numerical integration of (6) for different number concentrations the optimum concentration (c_{opt}) for a particle system where highest SHG signals can be obtained is theoretically accessible. However, an analytic expression for

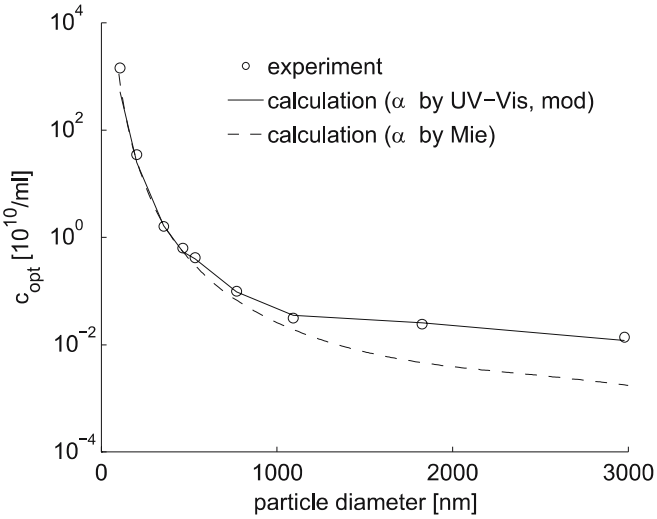

FIGURE 9 Comparison of the experimentally obtained optimal particle concentrations (*circles*) and the corresponding theoretical concentrations. The calculations were separately performed with theoretical values of α_ω by Mie (*dotted line*) and by UV-Vis (*solid line*) already modified for larger particles (by dividing by 3.5)

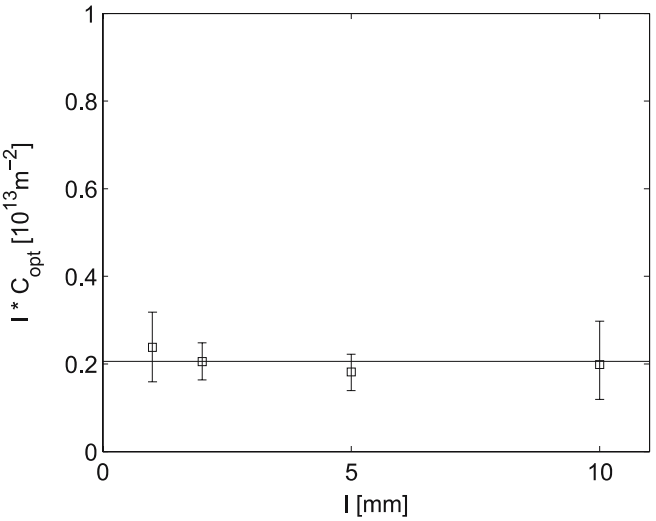

FIGURE 10 Verifying the constancy of the product lc_{opt} for 0.771-μm PS particles with MG

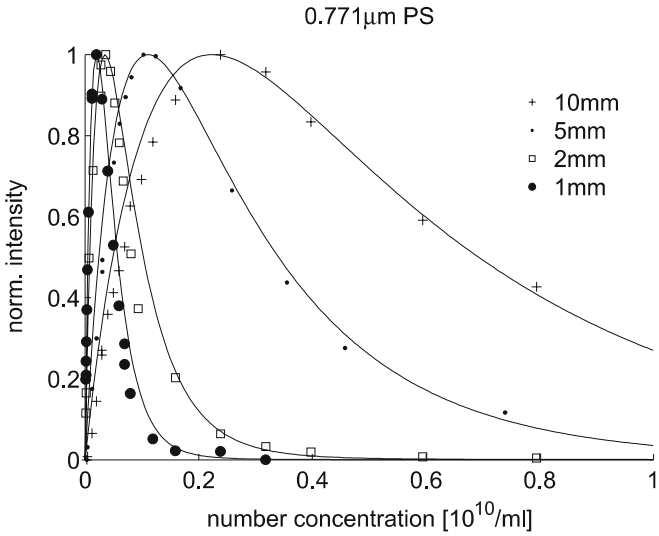

FIGURE 11 Verifying (6) for different path lengths with 0.771-μm PS particles with MG

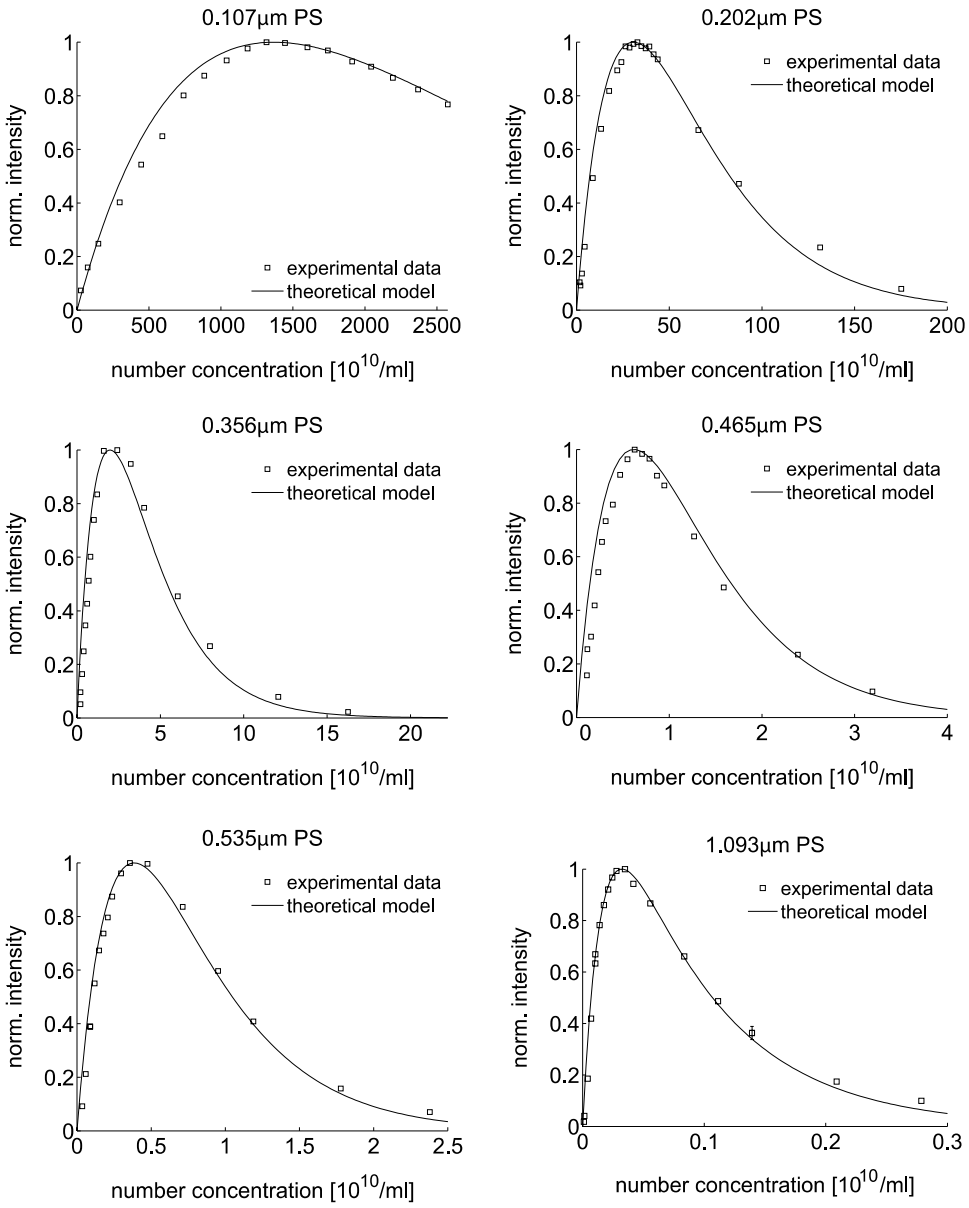

FIGURE 12 Comparison of the experimental and theoretical trends of the concentration dependence for the particles lower than 1.1 μm

this optimum concentration can also be derived: neglecting the factor $1/w(z)^2$ in (6) leads to an integral which can be solved analytically:

$$I_{2\omega}^{apr} = \beta^{*2} w_0^4 c \int_{z_0}^{z_1} \mathrm{e}^{-2\alpha_\omega c(z-z_0)} \mathrm{e}^{-\alpha_{2\omega}^* c(z_1-z)} \mathrm{d}z \,, \tag{7}$$

$$I_{2\omega}^{apr} = \frac{\beta^{**2}}{2\alpha_\omega - \alpha_{2\omega}} \left(\mathrm{e}^{-\alpha_{2\omega} cl} - \mathrm{e}^{-2\alpha_\omega cl}\right) , \tag{8}$$

where $l = z_1 - z_0$ is the cuvette length. In this case the changes in intensity with propagating distance z due to focusing will be neglected. Thus, the resulting equation will not be applicable to describe the absolute values of the SHG signal intensity (if β^* was known). Nevertheless, the behavior of the concentration dependence is not strongly affected for moderate focusing ($f > 100$ mm). The lens used in our experiments had a focal length of 100 mm. And, even for lower focal lengths at least the peak of the SHG intensity can be found at the same number concentration. Figure 8 demonstrates these assumptions, where the concentration behavior for different focal lengths calculated by (6) is illustrated besides the trend resulting from (8). Thus, differentiating (8) and solving the resulting homogeneous equation leads to an analytical expression for the optimal concentration:

$$c_{\mathrm{opt}} = \frac{1}{(\alpha_{2\omega} - 2\alpha_\omega)\, l} \ln\left(\frac{\alpha_{2\omega}}{2\alpha_\omega}\right) . \tag{9}$$

Figure 9 shows the optimal concentration calculated by (9) using the extinction coefficients obtained by the UV-Vis measurements (solid line) modified for the larger particles (by dividing by 3.5) as well as the calculated ones (by Mie theory). Good agreement between the calculated and the experimental values for the optimal concentration can be seen.

4.5 *Testing the model*

Corresponding to (9), the product of c_{opt} and the path length l should be constant. This assertion can be verified by ascertain experimentally the optimal concentration for the same suspension in cuvettes of different lengths. Figure 10 shows the result for the 0.771-μm particles. An approximately constant value for the different cuvettes can be seen. The concentration dependences for these particles in the different cuvettes are demonstrated in Fig. 11. The solid lines represent the calculated trends by (6), with the adapted values for the cuvette entrance (z_0) and exit (z_1). In these calculations the same value for t ($t = 6$) was used. Since the theoretical and the experimental trends coincide, another hint of accuracy for the model is given.

5 Conclusion and outlook

An investigation of the concentration dependence in colloidal SHG spectroscopy was presented. In this context a simple theory shows a high correspondence with the experimental data. Based on this model the trend of the SHG signal as a function of concentration can be predicted numerically. For the determination of the optimal concentration an analytical equation was derived. Due to this equation the optimal concentration depends only on the linear extinction coefficients and the optical path length (cuvette length). It shows the possibility of adapting the path length in an experiment where the suspension concentration is fixed due to external constraints, e.g. in technical processes for particle formation.

In future experiments the obtained insights have to be extended to different particle systems (consisting of different materials) and especially for particles with a certain size distribution. In the latter case the effective nonlinear susceptibility cannot be assumed as constant any more. The interesting question would be if a mean effective susceptibility (averaged over the different size fractions) can be used to apply the model derived here for such a system also. An amplification of our investigations in this context would be the determination of the effective nonlinear susceptibility for the monodisperse systems by fitting the experimental data applying (6) with β^* as the only fitting parameter. The thus obtained values would be a direct indication of the signal strength for the SHG light generated at the surface of particles with different sizes.

ACKNOWLEDGEMENTS The authors would like to thank the German Research Association (DFG) for their financial support (Project No. PE427/11-1).

REFERENCES

1 S. Mende, J. Schwedes, F. Stenger, W. Peukert, Powder Technol. **132**, 64 (2003)
2 C.T. Williams, D.A. Beattie, Surf. Sci. **500**, 545 (2001)
3 H. Wang, E. Borguet, E.C.Y. Yan, D. Zhang, J. Gutow, K.B. Eisenthal, Langmuir **14**, 1472 (1998)
4 H. Wang, E.C.Y. Yan, E. Borguet, K.B. Eisenthal, Chem. Phys. Lett. **259**, 15 (1996)
5 N. Yang, W.E. Angerer, A.G. Yodh, Phys. Rev. Lett. **87**, 103 902 (2001)
6 H.M. Eckenrode, H.L. Dai, Langmuir **20**, 9202 (2004)
7 H.M. Eckenrode, S.H. Jen, J. Han, A.G. Yeh, H.L. Dai, J. Phys. Chem. B **109**, 4646 (2004)
8 H. Wang, T. Troxler, A.G. Yeh, H.L. Dai, Langmuir **16**, 2475 (2000)
9 E.C.Y. Yan, K.B. Eisenthal, J. Phys. Chem. **103**, 6056 (1999)
10 H. Wang, E.C.Y. Yan, Y. Liu, K.B. Eisenthal, J. Phys. Chem. **102**, 4446 (1998)
11 Y. Liu, E.C.Y. Yan, X. Zhao, K.B. Eisenthal, Langmuir **17**, 2063 (2001)
12 E.C.Y. Yan, Y. Liu, K.B. Eisenthal, J. Phys. Chem. B **102**, 6331 (1998)
13 Y. Liu, J.I. Dadap, D. Zimdars, K.B. Eisenthal, J. Phys. Chem. **103**, 2480 (1999)
14 J.I. Dadap, J. Shan, T.F. Heinz, J. Opt. Soc. Am. B **21**, 1328 (2004)
15 J. Shan, J.I. Dadap, I. Stiopkin, A. Reider, T.F. Heinz, Phys. Rev. A **73**, 023 819 (2006)
16 Y. Pavlyukh, W. Huebner, Phys. Rev. B **70**, 245 434 (2004)
17 W.L. Mochan, J.A. Maytorena, Phys. Rev. B **68**, 085 318 (2003)
18 V.L. Brudny, B.S. Mendoza, W.L. Mochan, Phys. Rev. B **62**, 11 152 (2000)
19 S.H. Jen, H.L. Dai, Phys. Chem. Lett. B **110**, 23 000 (2006)